Received: 22 September 2022 | Revised: 15 March 2023 | Accepted: 24 March 2023

https://doi.org/10.1016/j.jtha.2023.03.042

ORIGINAL ARTICLE

Structures of factor XI and prekallikrein bound to domain 6 of high–molecular weight kininogen reveal alternate domain 6 conformations and exosites

Chan Li[1] | Awital Bar Barroeta[2] | Szu Shen Wong[3] | Hyo Jung Kim[1] | Monika Pathak[1] | Ingrid Dreveny[1] | Joost C. M. Meijers[2,4,5] | Jonas Emsley[1]

[1]Biodiscovery Institute, School of Pharmacy, University of Nottingham, Nottingham, UK

[2]Department of Molecular Hematology, Sanquin Research, Amsterdam, The Netherlands

[3]School of Pharmacy and Bioengineering, Keele University, Staffordshire, UK

[4]Amsterdam UMC, University of Amsterdam, department of Experimental Vascular Medicine, Amsterdam, The Netherlands

[5]Amsterdam Cardiovascular Sciences, Pulmonary Hypertension and Thrombosis, Amsterdam, The Netherlands

Correspondence
Jonas Emsley, Biodiscovery Institute, School of Pharmacy, University of Nottingham, Nottingham, NG7 2RD, UK.
Email: jonas.emsley@nottingham.ac.uk

Funding information
British Heart Foundation Programme Grant no. RG/12/9/29775 to J.E. and grant 1702 from the Landsteiner Foundation for Blood Research to J.C.M.M.

Abstract

Background: High–molecular weight kininogen (HK) circulates in plasma as a complex with zymogen prekallikrein (PK). HK is both a substrate and a cofactor for activated plasma kallikrein, and the principal exosite interactions occur between PK N-terminal apple domains and the C-terminal D6 domain of HK.

Objectives: To determine the structure of the complex formed between PK apple domains and an HKD6 fragment and compare this with the coagulation factor XI (FXI)-HK complex.

Methods: We produced recombinant FXI and PK heavy chains (HCs) spanning all 4 apple domains. We cocrystallized PKHC (and subsequently FXIHC) with a 31-amino acid synthetic peptide spanning HK residues Ser565-Lys595 and determined the crystal structure. We also analyzed the full-length FXI-HK complex in solution using hydrogen deuterium exchange mass spectrometry.

Results: The 2.3Å PKHC-HK peptide crystal structure revealed that the HKD6 sequence WIPDIQ (Trp569-Gln574) binds to the apple 1 domain and HK FNPISDFPDT (Phe582-Thr591) binds to the apple 2 domain with a flexible intervening sequence resulting in a bent double conformation. A second 3.2Å FXIHC-HK peptide crystal structure revealed a similar interaction with the apple 2 domain but an alternate, straightened conformation of the HK peptide where residues LSFN (Leu579-Asn583) interacts with a unique pocket formed between the apple 2 and 3 domains. HDX-MS of full length FXI-HK complex in solution confirmed interactions with both apple 2 and apple 3.

Conclusions: The alternate conformations and exosite binding of the HKD6 peptide likely reflects the diverging relationship of HK to the functions of PK and FXI.

KEYWORDS
factor IX, factor XI, factor XII, kininogens, prekallikrein

Manuscript handled by: Patricia Liaw

Final decision: Patricia Liaw, 24 March 2023

Chan Li and Awital Bar Barroeta contributed equally to this study.

1 | INTRODUCTION

Plasma prekallikrein (PK) and coagulation factor XI (FXI) act as master regulators of several cascades, including coagulation, fibrinolysis, complement activation, and inflammation (Figure 1A) [1–5]. PK and FXI are homologous and share 58% amino acid sequence identity with the unique feature of 4 tandem repeats of 90-amino acid apple domains at the N-terminus harboring exosites for substrates, cofactors, and receptors (Figure 1B) [6]. PK and FXI are serine proteases that circulate as a bound complex with their substrate high–molecular weight kininogen (HK). We have previously described the crystal structure for the inactive FXI zymogen and activated plasma kallikrein (PKa), revealing a large rotation of the apple domain disc upon activation [7,8].

The PK-HK complex [9] can be activated by a single cleavage from coagulation factor XIIa (FXIIa). The PK-HK complex can also undergo autoactivation in the presence of zinc ions and negatively charged polymers [10,11]. PKa performs double cleavage of HK to liberate the vasoactive peptide bradykinin, which binds the G-protein–coupled receptor B2R on endothelial cells, leading to activation of signaling events. Deficient regulation of the system is exemplified by the disorder hereditary angioedema, in which reduction of the natural inhibitor, serpin C1, or hyperactivated FXII results in excessive bradykinin generation and recurrent attacks of severe tissue swelling [12]. PK is currently being targeted as a novel means to treat diverse thrombotic and inflammatory disorders [13–18].

The mature polypeptide of HK is 626 amino acids in length with 6 domains (D1-D6); notably, D3 interacts with platelets, D4 harbors the bradykinin peptide, and D5 contains a histidine-rich region that binds to cell surfaces [19] (Figure 1B). The C-terminal D6 domain interacts with PK and is important for determining the selectivity of HK over low–molecular weight kininogen, which lacks D6 [8,19–21]. The cofactor function of HK is also thought to localize PK and FXI to the correct activated cell membrane. We sought to understand the molecular structures underlying how FXI and PK recognize HK. To this effect, we determined the crystal structure of the PK and FXI apple domains in complex with a HKD6 31-amino acid peptide, and these structures revealed alternate conformations of HKD6.

Essentials

- Factor XI (FXI) and prekallikrein (PK) form key exosite interactions with the D6 domain of high–molecular weight kininogen (HK).
- Structures of FXI and PK heavy chain (HC) complexed to an HKD6 peptide reveal exosite interactions.
- Both FXIHC and PKHC interact with the HK582-591 sequence FNPISDFPDT via the apple 2 domain.
- PKHC has a second exosite in the apple 1 domain, whereas FXIHC utilizes an apple 2/3 domain pocket.

2 | METHODS

2.1 | Protein purification, crystallization, and structure determination

A gene encoding human PK (gene *KLKB1*) was cloned into the pMT puro vector using BglII and MluI restriction sites with a 6 histidine tag at the N-terminus after the immunoglobulin-binding chaperone protein secretion signal for expression using the *Drosophila* expression system (Invitrogen). The PK heavy chain (HC) construct spanning residues 1 to 359 was prepared by introduction of a stop codon in the full-length PK cDNA.

Drosophila S2 cells were grown in Schneider's drosophila medium supplemented with 10% fetal calf serum at 28 °C, and transfection was performed using calcium phosphate. Cells were grown for an additional 48 hours before selection with puromycin to establish stable cell lines. Proteins were expressed in serum-free Express Five insect culture medium (Gibco) and the cells were harvested 6 days after induction with 0.5 mM Cu_2SO_4. Protein purification was performed using a Capto S column followed by a Ni-Sepharose affinity column and a Superdex 200 gel filtration column (GE healthcare) (Supplementary Figure S1).

PKHC at a concentration of 19.6 mg/mL in buffer 20 mM Tris-Cl, 150 mM NaCl, pH 8.0 was mixed with a 31-amino acid synthetic peptide (Biomatik) derived from substrate HK spanning residues Ser565-Lys595 (termed HKpep1) with a 1:5 molar ratio. This PKHC-HKpep1 peptide complex crystallized in the Morpheus screen containing 0.1 M amino acids mixture, 0.1 M buffer 3, pH 8.5, 25% PEG MME 500, and PEG 20000. Data were collected on beamline I04 to 2.3Å for the PKHC–HKpep1 complex, and were processed and reduced using XDS and the CCP4 suite [22]. The structures were determined by molecular replacement with PHASER [23] using coordinates from the FXI heavy chain (Protein Data Bank code 2F83) [7]. Models were built with COOT [24] and refined with REFMAC. Data collection and refinement statistics are summarized in the Table. Figures were generated using PyMOL. HKpep1 interactions with PK were generated using LigPlot+ software [25]. FXIHC was purified using similar methodology as PKHC. FXIHC was mixed with the same HKpep1 in a 1:5 molar ratio and crystallized in the presence of 100 mM Tris and 1.8 M ammonium sulfate. The FXIHC–HKpep1 complex structure was also determined by molecular replacement as described above.

2.2 | Cell culture, protein expression, and protein purification for HDX–MS

FXI-wild-type (WT) cDNA with a Cys11Ser mutation was introduced in pCDNA3.1. FXI-N72QN108Q was prepared from FXI-WT by Quikchange (Agilent) mutagenesis. Sequence analysis was used to

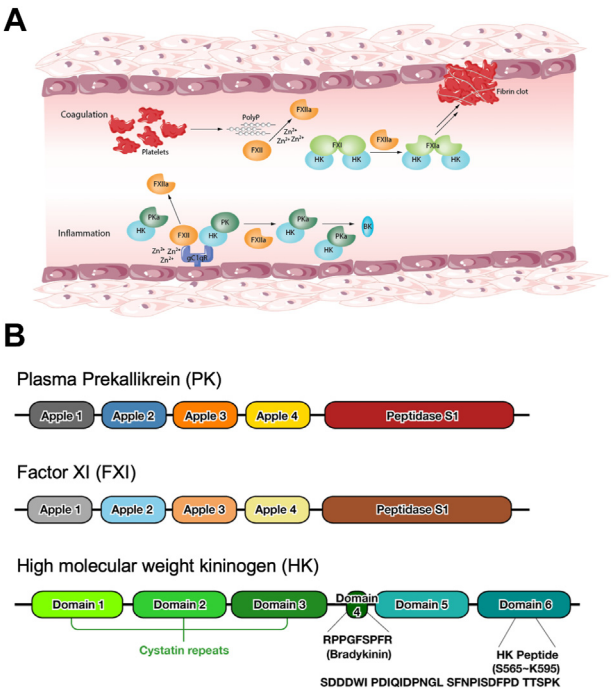

FIGURE 1 Structure and function of the contact system and FXI. (A) Schematic overview of the contact factors PK, FXII, HK, and FXI involvement in coagulation (top) and inflammation (bottom) pathways. Assembly of the contact system generates PKa, FXIIa, and BK on the surface of endothelial cells (bottom). FXIIa activates plasma coagulation cascades via FXI (top). (B) Schematic diagrams showing the domain organization of FXI, PK, and HK. FXI, factor XI; FXII, factor XII; BK, bradykinin; HK, high–molecular weight kininogen; PK, prekallikrein.

confirm the introduced mutations. FXI-WT was stably transfected in HEK293 cells (ATCC) using calcium precipitation. DMRIE-C (Invitrogen) was used for transfection of DNA into HEK293 cells. Medium (DMEM F12, Lonza) with 5% fetal calf serum was used to expand and grow cells. For expression, FXI-WT was grown in a Cell Factory (6320 cm^2, Thermo Fisher Scientific) and FXI-N72QN108Q in a TripleFlask (500 cm^2, Thermo Fisher Scientific). At confluence, serum-free medium (Opti-MEM I reduced serum medium with Glutamax supplement, Gibco) was added and collected every 48 to 72 hours. FXI was purified from expression medium using a peptide IV column after concentrating the collected medium over an artificial kidney (Fresenius Medical Care). The peptide IV column was eluted with 100 mM citrate pH 5.0, 1 M NaCl, and 10 mM EDTA. The eluent was checked for contamination with FXIa with chromogenic substrate S2366 (Chromogenix). Contaminating enzymes, including FXIa, were eliminated by treatment with serine protease inhibitor DFP until chromogenic activity was absent. FXI-WT was dialyzed against 10 mM HEPES (pH 7.5, containing 0.5 M NaCl, and stored at −80 °C. FXI-N72QN108Q was dialyzed against 10 mM HEPES, pH 7.5, containing 0.15 M NaCl and stored at −80 °C. The concentration of recombinant protein was determined by measuring the absorbance at 280 nm using the extinction coefficient for FXI (13.4), and the purity was checked by SDS-PAGE before and after deglycosylation with PNGase F (Supplementary Figure S2).

2.3 | Hydrogen deuterium exchange mass spectrometry

Protein samples (2 μM FXI-N72QN108Q or 2 μM FXI-N72QN108Q with 6 μM HK; Enzyme Research Laboratories) were placed in a LEAP PAL pipetting robot (LEAP Technologies,). Samples were diluted 10 times in binding buffer (10.47 mM HEPES pH 7.4, 150 mM NaCl, and 7.35 mM $CaCl_2$ in 98% D_2O), resulting in a final buffer composition of 9.9 mM Hepes pH 7.24, 150 mM NaCl, 6.6 mM $CaCl_2$, and 0.2 mM NaAc HCl, and samples were incubated for 10, 30, 100, 300, 600, or 1000 seconds at 24 °C. Incubation with a binding buffer containing H_2O instead of D_2O was used as reference. Deuterium exchange was quenched by mixing the sample 1:1 with quenching solution (1 g TCEP-HCl dissolved in 2 mL 2 M Urea, pH 2.5) for 1 minute at 4 °C. The sample was digested by passing it over a Poroszyme Immobilized Pepsin Cartridge with an isocratic flow of 5% acetonitrile and 0.1% formic acid for 5 minutes at 4 °C. After collection on a trap (Acclaim Guard Column. 120, C18, 5 μm, 2.0 × 10 mm), the peptides were washed for 30 seconds at 4 °C. Subsequently, peptides were eluted and passed over a C18 column (Hypersil Gold C18: 30 mm length, 1 mm diameter, particle size 1.9 μm, Thermo cat #25002-031030) using a gradient from 0.08% to 64% acetonitrile at 50 μL/min at 4 °C. Peptides were injected online into an LTQ Orbitrap-XL operating in positive mode. To identify peptides and their retention times, peptides were fragmented by collision-induced dissociation.

2.4 | Hydrogen deuterium exchange data analysis

Sequence and retention times of nondeuterated peptides were analyzed with PEAKS (PEAKS 7.0, Bioinformatics Solution Inc). Deuterated peptides were analyzed using HDExaminer 2.2.0 (Sierra Analytics), which calculated the deuterium uptake of peptides within 1 minute retention time. Identified peptides were assessed manually. Peptides were discarded if not accurately detected in at least half of the measurements for both compared samples. The percentage of deuterium uptake (%D) was calculated for each peptide relative to the theoretical maximal amount of deuterium incorporation. The presented HDX data consist of the mean value and corresponding SDs of 3 to 5 independent experiments calculated individually for 6 different incubation times (10, 30, 100, 300, 600, or 1000 seconds). Data points with an SD greater than 5% were not included. Results were visualized in a 3D protein model using PyMOL (Schrödinger).

2.5 | Surface plasmon resonance binding studies

PKHC or full-length recombinant PK active site mutant (PKS578A) were immobilized onto sample cells on a COOHV sensor chip using an amine coupling kit (Cytiva), and experiments were performed on a SensiQ Pioneer instrument. The running buffer used for all experiments was 10 mM HEPES pH 7.4, 150 mM NaCl, 50 μM EDTA, and 0.005% P20. The analytes (HK peptides) were also injected over the

TABLE Data collection and structure refinement statistics.

Sample	PKHC-HKpep1	FXIHC-HKpep1
Data collection		
Space group	$P2_1$	$P6_122$
Cell dimensions		
a, b, c (Å)	55.5, 68.3, 120.3	87.3, 87.3, 629.6
α, β, γ (°)	90, 96.6, 90	90, 90, 120
Wavelength (Å)	0.9795	0.9795
Resolution (Å)	2.3	3.2
*R*merge[a]	0.129 (0.683)	0.075 (0.269)
$I/\sigma I$	7.6 (1.7)	16.5 (6.4)
Completeness (%)	99.4 (98.4)	94.9 (100)
Multiplicity	3.4 (3.4)	10.8 (11.3)
CC ½	0.987 (0.597)	0.994 (0.993)
Unique reflections	38 741	19 451
Structure refinement		
R_{work}	0.199 (0.253)	0.251 (0.284)
R_{free}	0.203 (0.243)	0.254 (0.28)
Overall B factor (A^2)	34	61
RMS deviations		
Bond length (Å)	0.007	0.007
Bond angle (°)	1.2	1.16
Ramachandran statistics[b]		
Favored (%)	98.0	93.1
Allowed (%)	2.0	6.8
Outliers (%)	0	0.1

CC ½, Pearson correlation coefficient; FXIHC, factor XI heavy chain; PKHC, prekallikrein heavy chain; RMS, root-mean-square.
[a] Numbers in parentheses are for the highest resolution shell.
[b] Ramachandran statistics were calculated using Molprobity.

PKHC surface with 10 concentration points in a series, ie, 50, 40, 25, 20, 12.5, 6.25, 3.125, 1.56, and 0 μM. To assess any nonspecific binding, the analytes (HK peptides) were also injected over an empty reference flow cell. The regeneration buffer was 10 mM glycine pH 2.5. For kinetic analyses, the responses were plotted against the analyte concentration and fit to a 1:1 (A + B = AB) or 1:2 (A + 2B = AB1 + AB2) binding model using QDat analysis software (SensiQ Technologies, Inc).

3 | RESULTS

3.1 | PKHC–HKpep1 complex structure

Previous studies have mapped PK binding to HK residues located at the C-terminal D6 domain spanning residues Ser565-Lys595 [26]. In addition, a variety of different techniques demonstrated the importance of the PKHC and particularly apple 2 domain to the PK-HK interaction [21]. We thus sought to determine the PKHC crystal structure in complex with a 31-amino acid synthetic peptide derived from the HKD6 domain sequence (termed HKpep1). We expressed PKHC and purified recombinant protein from the media using a histidine tag (residues 1-359 described in the methods [Section 2.1]). PKHC was mixed with a 1:5 ratio of HKpep1, and the complex structure was solved to 2.3 Å resolution (Table). Figure 2A shows the N-terminal sequence WIPDIQ (Trp569-Gln574) interacting with the apple 1 domain (gray) and the C-terminal region FNPISDFPDT (Phe582-Thr591) interacting with the apple 2 domain (blue). The intervening HK-peptide residues Ile575-Asp581 are not observed in the electron density and are assumed to be flexible (dashed green line in Figure 2A).

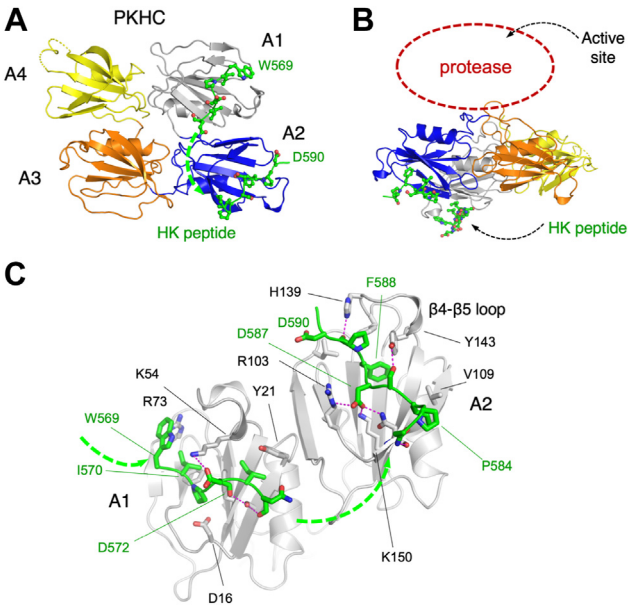

FIGURE 2 PKHC-HK peptide complex structure. (A) Cartoon diagram of the PKHC-HK peptide structure with the apple domains colored A1 (gray), A2 (blue), A3 (orange), and A4 (yellow). The bound HK peptide is shown in green as sticks with residue numbers labeled. Only HK residues W569-Q574 and F582-T591 are observed in the bound peptide structure with the intervening residues 574-581 and 592-599 assumed to be flexible (green dashed line). (B) The same structure is shown as a 90° rotation illustrating the flat structure of the 4 apple domains and the opposing positions of the protease domain active site (red dotted line). (C) Closeup view of a cartoon diagram of PK apple 1 and apple 2 domains (gray) with the HK-fragment peptide colored green and electrostatic interactions are shown as purple dotted lines and the path of the connecting peptide a dashed line (green). HK, high–molecular weight kininogen; PKHC, prekallikrein heavy chain.

The WIPDIQ peptide forms contacts exclusively with the PK apple 1 domain via the 2 isoleucine side chains; the first Ile570 inserts into a major hydrophobic pocket formed between the β-sheet and β4-β5 loop (PK residues Phe11, Phe59, Leu44, Ile49) shown in Figure 3B, C. The second Ile573 side chain inserts into an adjacent minor pocket formed between 2 aromatic side chains of PK residues Tyr21 and Phe59. The

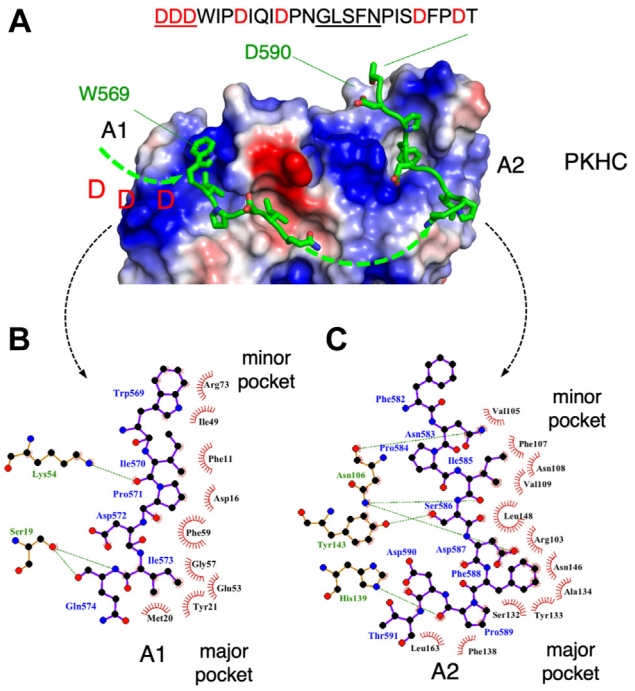

FIGURE 3 PKHC charge surface. (A) Charged surface representation shown for the PKHC apple domains (blue=positive, red=negative) and the HK-peptide structure is shown as sticks in green. The HK peptide sequence is shown with negatively charged residues in red and underlined residues are not observed in the structure. (B) Schematic diagram of the HK WIPDIQ peptide bound to the PK A1 domain with hydrogen bonds shown as green dotted lines (Ligplot). (C) Schematic diagram of the HK NPISDFP peptide bound to the PK A2 domain with hydrogen bonds shown as green dotted lines (Ligplot). HK, high–molecular weight kininogen; PKHC, prekallikrein heavy chain.

HK Asp572 side chain remains surface exposed, forming a salt bridge to PK Lys54 from the rim of the major pocket and HK Pro571 packs against Phe59 and buries the PK Asp16-Lys61 salt bridge. The acidic residues Asp566, Asp567, and Asp568 are not observed in the electron density (labeled as DDD in Figure 3A). Previous biochemical studies measuring bradykinin generation in a cell-based assay showed that HK Asp566-Asp567-Asp568 contributes to a productive enzyme complex with PK [27]. There are positively charged amino acids (Arg13, Lys70, His72, and Arg73) in the region that may form longer range electrostatic interactions with Asp566-Asp567-Asp568.

From the C-terminal HK NPISDFPDT sequence, the HK DFP motif residue Phe588 is fully buried in a major pocket of the apple 2 domain, forming extensive contacts with side chains from residues Phe138, Tyr143, Asn146, Ser132, Leu148, and Ala134. The DFP Asp587 carboxylate forms a hydrogen bond to the PK Asn106 side chain and a salt bridge to Arg103 on the rim of the pocket (Figure 3C). The DFP Pro589 ring is pinched on either side by sidechain interactions with His139 and Tyr143 from the β4-β5 loop. A second interaction site at a minor pocket occurs from the HK residue Ile585 contacting residues Phe107, Asn108, and Val109. The structure reveals that the HK Asn583 side chain forms an internal hydrogen bond and contacts the main chain carbonyl of PK Asn106, which occurs at the abrupt change in direction of the HK polypeptide chain pointing it toward the apple 1 domain in a bent double conformation.

A comparison of the apple 1 and apple 2 HK peptide complex structures reveals a number of common features that are maintained in the 2 sets of interactions despite the polypeptide chain direction being reversed (Figure 3A–C). Both utilize a major hydrophobic pocket, which is topologically at approximately the same position formed between the β-sheet and β4–β5 loop and both use a direct salt bridge to the peptide aspartate side chain from a PK lysine/arginine residue on the rim of the major pocket. In each case, the HK peptide binding partially buries 2 salt bridges from the apple domain. The minor pocket interacts with an isoleucine side chain from the HK peptide in both cases, although the position of this pocket is shifted closer to the major pocket in apple 1 compared with apple 2.

3.2 | Surface plasmon resonance binding analysis of the PKHC HKPep1 binding

To extend upon previous studies [26] and precisely quantitate the interaction of PKHC with the HKpep1 sample used in the crystallization experiments, we developed a surface plasmon resonance (SPR) assay with next-generation SensiQ Pioneer instrument. In this binding assay, either PKHC or full-length recombinant PK active site mutant (HisPKS578A) described previously [28] was immobilized on the surface of the chip and the analyte consisted of HKD6-derived peptides. We injected a series of peptides including HKpep1, together with shorter peptides derived from the sequence that binds to the apple 2 domain (HKpepC) and the apple 1 domain (HKpepN), respectively.

The HKpep1 and 2 peptides resulted in high-quality binding curves which were fitted using the SensiQ software QDat as a 2-site binding model, and derived K_D and error values are presented in Supplementary Table S1. The tighter binding value of K_{D1} 57.8 ± 4.8 nM, for PKHC may represent HKpep1 binding to both apple 1 and apple 2 with the weaker K_{D2} 2.9 ± 0.13 μM value representing binding to just the apple 2 domain. HKpep1 is equivalent to HK peptide IV (Tait et al. [26]), and the K_{D1} of 57.8 nM is in approximate agreement with the published value of 20 nM measuring PK binding to HK peptide IV. Similar values were obtained for full-length PKS578A with K_{D1} = 83.8 ± 6.9 nM and K_{D2} = 4.4 ± 0.3 μM, although both values have slightly reduced binding, which may reflect the presence of the protease domain modifying the apple domain structure.

The binding curves for the shorter peptide fragments HKpepC that binds the apple 2 domain could be fit as a single-binding event and reveals a K_D of 40.2 ± 3.4 μM for PKHC and a value of 31.4 ± 3.4 μM for PKS578A. HKpepC is equivalent to HK peptide II (Tait et al. [26]) and their derived value of 6 μM is similar to 31 μM. Overall binding of the shorter HK peptides that interact with a single apple domain has 1000-fold reduced binding compared with the whole HKpep1, which binds 2 apple domains. Binding curves for HKpepN could not be fit and a peptide from the far C-terminal region of HK (HKCterm) was also tested for binding as a negative control, and no binding curves were obtained.

3.3 | FXIHC–HKPep1 complex structure

As FXI is a dimer and PK is a monomer, we anticipated that there may be differences in the way FXI formed interactions with HK compared with PK. We thus expressed the FXI apple domains (FXIHC) using a similar construct and protocol to the PK apple domains. Nonreducing SDS-PAGE confirmed that a disulfide-linked FXIHC dimer was formed [7]. The FXIHC–HKpep1 structure reveals a straightened HKpep1 structure that interacts with the apple 2 and 3 domains, as illustrated in Figure 4A, B. As expected, the C-terminal HK peptide sequence NPISDFPDT interacts with the FXI apple 2 domain [29]. Unexpectedly, the N-terminal sequence extends toward the apple 3 domain instead of the apple 1 domain, as observed in PKHC. The HK-peptide residues Leu580 and Phe582 form interactions with a small pocket at the interface between the FXI apple 2 and 3 domains created by residues Tyr107, His127, His151, and Glu243 (Figure 4D). As with the PKHC–HKpep1 complex structure, we did not observe HK residues Asp566, Asp567, and Asp568 in the FXI–HKpep1 peptide complex electron density, and residues from the preceding HK sequence QIDPNG were also not well resolved. This N-terminal part of the HK peptide is in close proximity to FXI residues Lys252, Lys253, and Lys255, which forms the apple 3 domain anion-binding site and thus long-range electrostatic interactions may contribute to the binding [30]. The discovery of a HK-binding pocket between the FXI apple 2 and 3 domains is novel and yet it remains to be determined how additional interactions from HKD6 beyond the HKpep1 peptide described here contribute to FXI binding and whether glycosylation of HKD6 plays a role [26].

3.4 | HDX–MS analysis of the FXI-HK complex

To investigate the FXI interaction with HK using the full-length proteins, we next moved on to analyze the binding in solution using HDX–MS, which was performed largely as described previously [31]. Fragmentation was first performed with FXI-WT. This fragmentation did not cover peptides in the proposed binding site of HK. This could be due to glycosylation, which disturbs peptide detection by MS. To overcome this, an FXI variant lacking this glycosylation was prepared. Additionally, a FXI N72Q mutation was introduced to obtain coverage of the thrombin-binding site on FXI to assess whether HK interaction with FXI influences the deuterium uptake in this region. When fragmentation was repeated with FXI-N72QN108Q, an increased protein sequence coverage was observed, mainly around the 2 glycosylation sites (Supplementary Figures S3 and S4). Therefore, the binding analysis was continued with the FXI-N72QN108Q mutant.

Deuterium uptake of FXI-N72QN108Q in the absence or presence of HK was analyzed after incubation with D_2O for 6 different time intervals (10, 30, 100, 300, 600, and 1000 seconds). This resulted in a final coverage of 91% of the FXI sequence totaling 183 peptides. Deuterium uptake remained unaltered after introduction of HK for most but 3 discrete regions, which showed a reduction in deuterium uptake (Figure 5A, Supplementary Figures S3 and S4). The first region is located in the apple 2 domain (FXI residues 101-107, peptide DMKGINY,

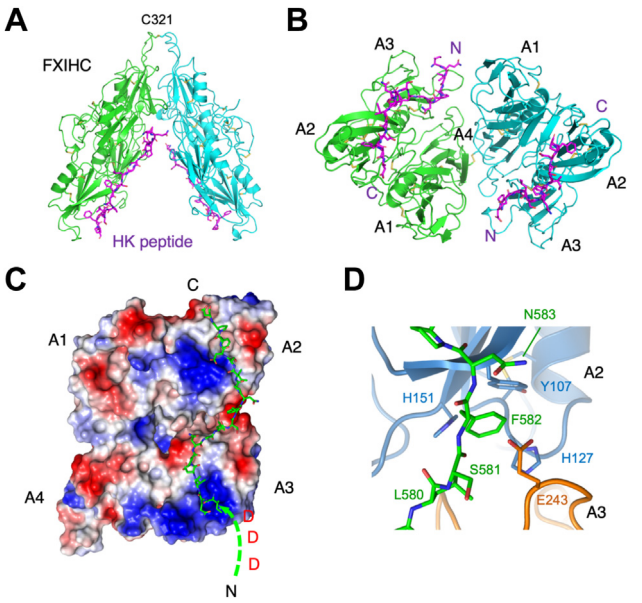

FIGURE 4 FXIHC-HK peptide complex structure. (A) Cartoon diagram of the dimeric FXIHC-HK peptide structure with the apple domains colored green and cyan for each monomer. The bound HK peptide residues W569-T591 are shown in purple as sticks. (B) The same FXIHC-HK structure is shown as a 90° rotated view. (C) Charged surface representation shown for the FXIHC apple domains (blue=positive, red=negative) and the HK-peptide structure is shown as sticks in green. The HK peptide sequence is shown with negatively charged residues in red, and underlined residues are not observed in the structure. (D) Closeup view of hydrophobic HK residues L580 and F582 interacting with a pocket between the FXI A2 (blue) and A3 domains (orange) with key residues shown as sticks. FXI, factor XI; FXII, factor XII; BK, bradykinin; HC, heavy chain; HK, high–molecular weight kininogen; PK, prekallikrein.

Figure 5A, B), and the second region in the apple 2 domain affected by HK is centered around the amino acids ATRQFPSL (FXI residues 134-141) (red in Figure 5A, B). Lastly, FXI amino acids LKTSESGLPST (residues 239-249, red in Figure 5B), located in the apple 3 domain show reduced deuterium uptake in the presence of HK (Figure 5A). This corroborated a location of the HK-binding site in FXI apple 3 from the crystal structure and that FXI apple 1 does not bind HK. A comparison of the apple 1 domain structures of FXI and PK shown in Figure 6A reveals that a different FXI β4-β5 loop conformation coupled with key amino acid changes significantly alters the shape of the FXI apple 1 β-sheet pocket such that it no longer forms interactions with HK.

4 | DISCUSSION

We report the first crystal structure of PKHC in complex with a 31-amino acid HKD6 peptide revealing 2 HK motifs NPISDFP and WIPDIQ interacting with pockets in the PKHC apple 1 and apple 2 domains, respectively. A second crystal structure of FXIHC in complex with the same peptide revealed similar interactions of the NPISDFP

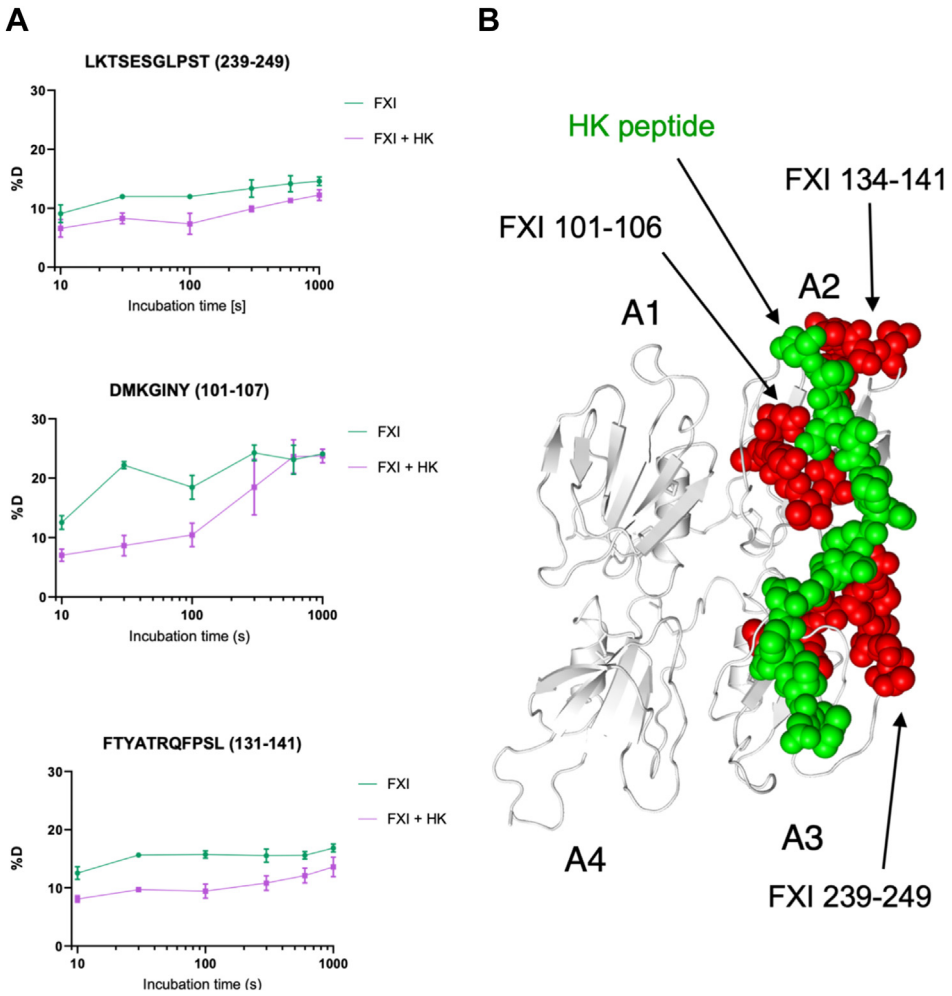

FIGURE 5 Hydrogen deuterium exchange mass spectrometry (HDX–MS) characterization of FXI and FXI-HK complex. (A) Deuterium uptake graphs of regions affected by binding of HK to FXI. Residues 101-107 (DMKGINY) and residues 134-141 (ATRQFPSL) in the A2 domain, and residues 239-249 (LKTSESGLPST) in the A3 domain show reduction in deuterium uptake upon binding to HK. (B) Representation of the peptide regions (red) in FXI affected by HK binding. HK peptide is depicted in green. FXI, factor XI; HDX–MS, hydrogen deuterium exchange mass spectrophotometry; HK, high–molecular weight kininogen.

sequence with the apple 2 domain but no interaction with the apple 1 domain. Instead, a unique FXIHC pocket located between the apple 2 and 3 domains forms an additional interaction with the central HKD6 sequence LSFN.

4.1 | Apple domain ligand recognition comparisons

We compared the PKHC-HK peptide complex structures with previously reported apple domain ligand complexes [32] and found unexpected similarities in the HK peptide DFP tripeptide ligand recognition of the PK apple 2 domain with microneme protein SML-2 PAN domain recognition of 1-thio-β-D-galactose [33]. Figure 6B–D shows the major pocket of the PK apple 2 domain and the Lys150 (green) forms a salt bridge to HK Asp587 (orange) bound and in the same orientation for comparison the microneme protein SML-2 from the parasite *Sarcocystis muris* where Lys59 (green) forms hydrogen bonds to the O3 and O2 hydroxyl groups of 1-thio-β-D-galactose. This establishes a conserved principle of ligand recognition for the PAN domain β-sheet via interactions with a major pocket involving a partially buried lysine residue on strand β5 directly contacting the ligand. The PK apple 2 domain Lys150 residue is present in the same position of the β5 strand in all PK and FXI apple domains (except PK apple 4 domain where the residue is Arg). The expansion of the size of the PK apple 1 and apple 2 domains major pocket by elaboration of the β4-β5 loop and the addition of the minor pocket allows the PK and FXI apple domains to recognize peptides spanning ~6 amino acids.

Our data also show that in FXI, but not PK, a pocket formed between the apple 2 and 3 domains is utilized to interact with the HK peptide (Figure 4D). Figure 6E shows a superposition of the PKHC-HKpep1 and FXIHC-HKpep1 structures in the region of HK residue Phe592 showing FXI pocket residues His151 and His127 are not conserved in PK. Substitutions of FXI His151 with the bulkier Tyr151 (PK) and His127 for Arg127 (PK) effectively filled in the pocket with the PK Arg127 guanidinium forming a cation–Pi interaction with the Tyr151 sidechain excluding HK residue Phe592 from forming interactions with PK.

4.2 | FXIHC conformational differences compared with FXI zymogen

The FXIHC-HK peptide structure was compared with the available FXI full-length zymogen crystal structure. Figure 6F shows 2 large,

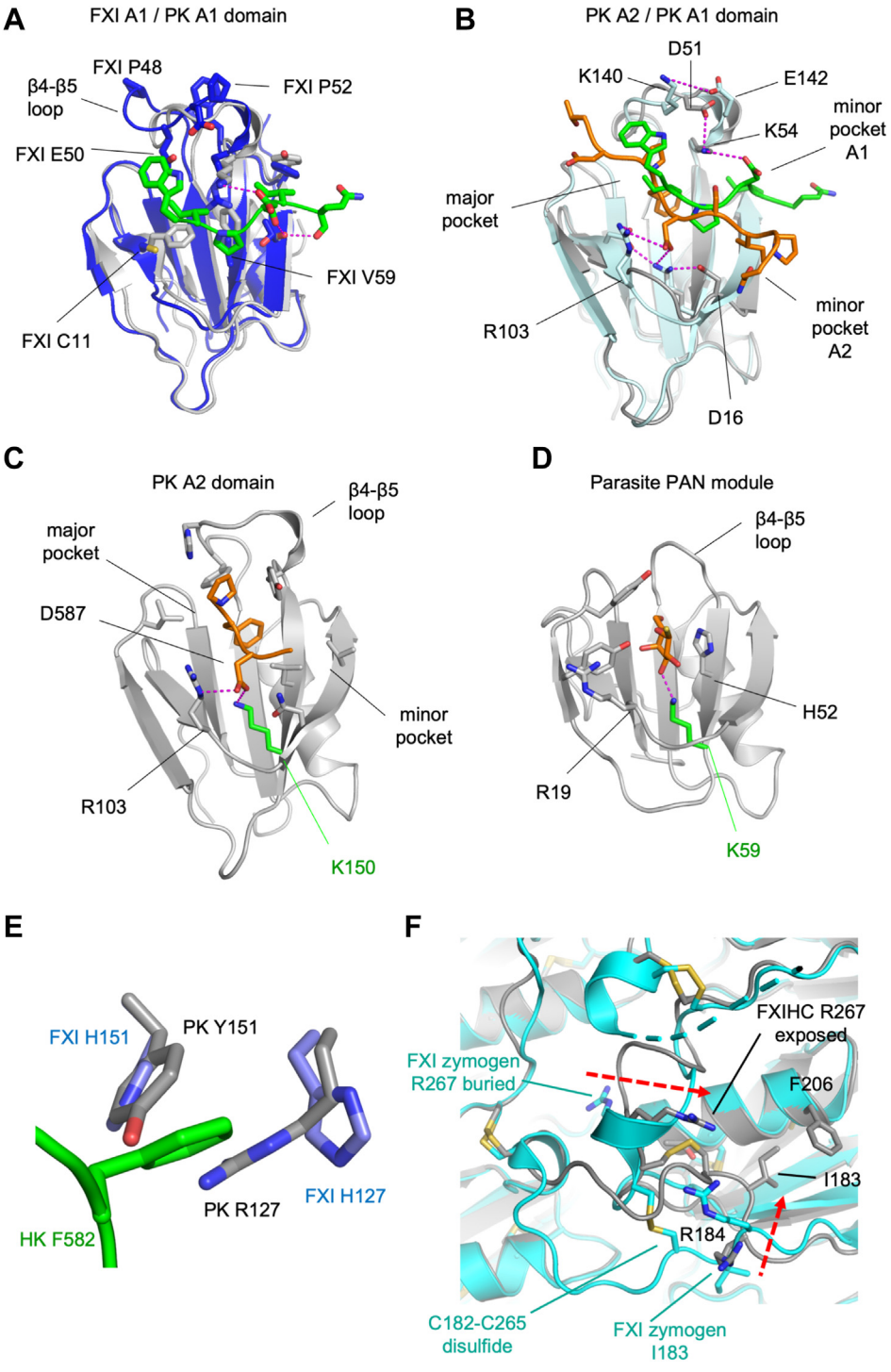

FIGURE 6 Comparison of apple domain ligand interactions and conformation change. (A) FXI A1 (dark blue) and PK A1 (gray) domains shown as cartoon diagrams superposed with PK bound HK peptide (green) as sticks. Differences in the FXI A1 domain structure are highlighted which likely preclude binding to the HK peptide. (B) PK A1 (light blue) and A2 (gray) domains shown as cartoon diagrams superposed with bound HK peptides as sticks. (C) Cartoon diagram of PK A2 (gray) domain illustrating K150 (green) coordinates the HK D587 carboxylate (orange) presented in the same orientation as (D) SML-2 PAN apple domain recognition of 1-thio-β-D-galactose (orange) with equivalent K59 shown in green. (E) HK residue F582 is shown as sticks (green) interacting with pocket residues H151, H127 from the FXI A2 and A3 domains. These 2 residues are not present in the PKHC structure and are replaced by bulkier Y151, R127 effectively filling the pocket. (F) Cartoon diagram showing a superposition of the FXIHC structure (gray) with the equivalent FXI zymogen crystal structure (cyan) reveals loop remodeling in the region of the A3 domain (red dashed arrows). Residue R267 (gray) from FXIHC is raised and becomes surface exposed compared with the equivalent residue in FXI (cyan), which is buried. Disulfides are in yellow. The loop structure connecting the A2 and A3 domains also flips toward the center of the disc bringing R184 into proximity to R267. Red arrows indicate the direction of loop movement from the FXI zymogen to the FXIHC structure. FXI, factor XI; HC, heavy chain; HK, high–molecular weight kininogen; PKHC, prekallikrein heavy chain.

concerted changes are that (i) loop residues 266-272 rearrange and flip Arg267 onto the surface bringing it into proximity to Arg184, (ii) residues 177 to 181 alter in conformation such that the Cys182-Cys265 disulphide moves 6 Å toward the α-helix residues Thr213 and Phe206. Increased exposure of residues on the upper surface of the apple 3 domain has been previously proposed to occur in FXIa to regulate binding to substrate FIX [24,34]. Here it was shown that FXIa has an exosite for the FIX Gla domain involving residues 183 to 185 from the FXIa apple 3 domain, which is cryptic in the FXI zymogen [35–37]. Consistent with this, the FXI zymogen structure shows that Arg184 is buried and forms a salt bridge with Asp488 from the catalytic domain, rendering it unavailable for binding to the FIX Gla domain [7,24].

We have previously described the crystal structure for the inactive dimeric FXI zymogen and the active form plasma kallikrein (PKa), revealing a large rotation of the apple domain disc when the 2

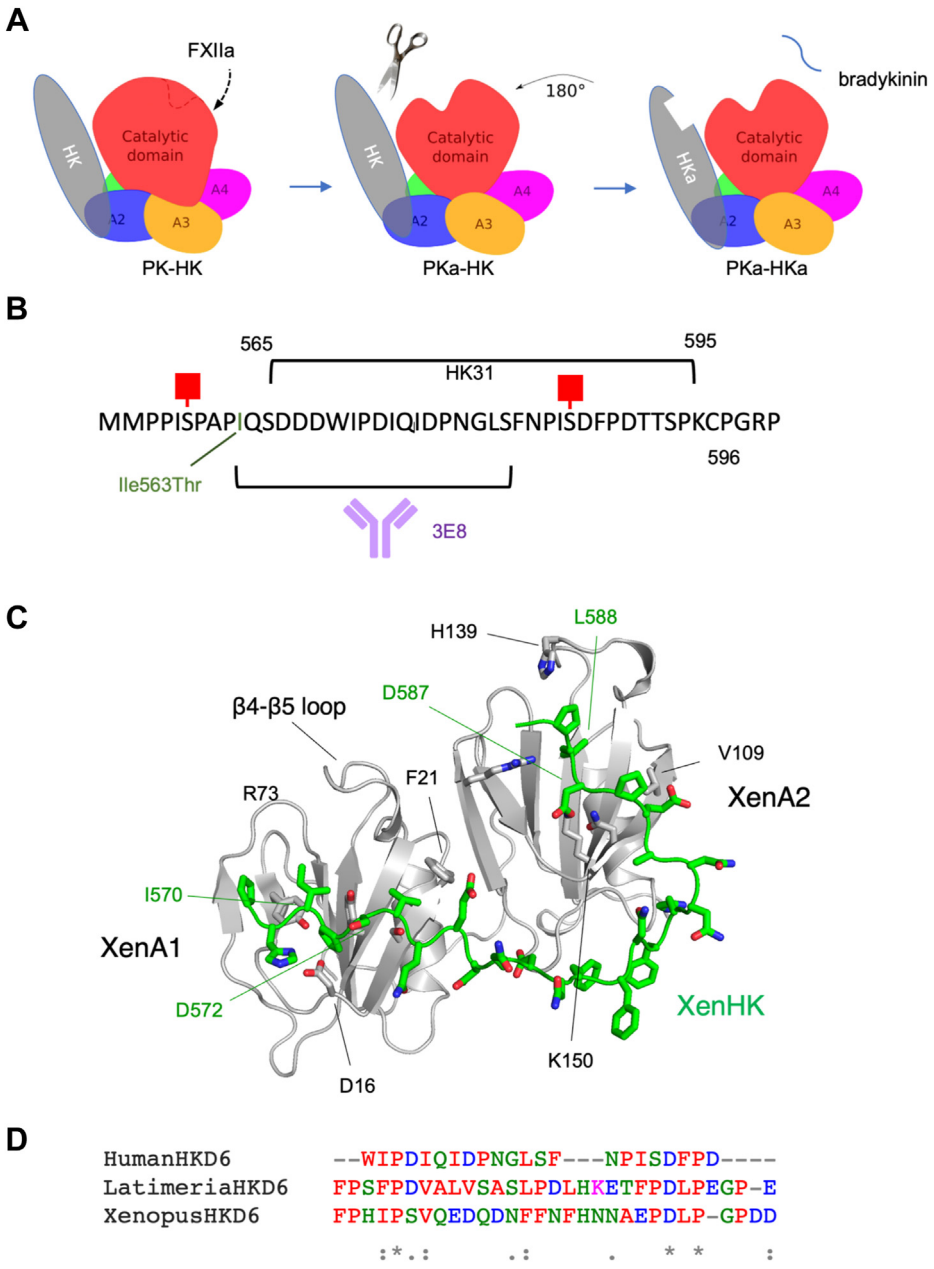

FIGURE 7 PKHC-HK structure, function, and evolution. (A) A schematic diagram of the PK zymogen monomer bound to HK via the A1 and A2 domains (left). Cleavage of PK by FXIIa generates PKa and a reorientation of the protease domain occurs by 180° relative rotation to the apple domains (middle), which enables cleavage of HK to form bradykinin and HKa (right). (B) Sequence of HKD6 in the region of the PK-binding site with O-glycan sites annotated (red boxes) as well as the function-blocking monoclonal antibody 3E8-binding site. The location of the common missense HK mutation Ile563Thr linked to venous thrombosis in humans is indicated. (C) Cartoon diagram showing an Alphafold model of Xenopus PK A1 and A2 domains interacting with XenHK. (D) Sequence alignment for HKD6 HKPep1 sequence derived from different species, *Xenopus laevis*, *Latimeria* chalumnae, and Human. Conserved residues are indicated as a star at the bottom. FXIIa, factor XIIa; HK, high–molecular weight kininogen; PKHC, prekallikrein heavy chain.

structures were compared [7,8]. As FXI and PK are unusual examples of a zymogen protease already bound to its substrate, we speculated that the structure we observed was designed to position the disc of the apple domains such that they act as a physical barrier to keep the bound HK substrate at "arm's length" away from the active site. Disruption of this arrangement in the PK-HK zymogen can be brought about by FXIIa cleavage and disc rotation, as we have reported previously (Figure 7A).

4.3 | Functional importance of the HKD6 interaction with PK and FXI

The functional importance of the PK apple 2 domain β4-β5 loop interaction with HK has been highlighted by previous data showing that a PKa autolytic inactivation cleavage occurs here at the Lys140-Ala141 bond, which reduces HK binding by 10-fold [19]. The wider role of the HKD6 interaction with PK/FXI has been probed using synthetic HKD6 peptides (termed HK31, WIP27) showing they block binding of PK to endothelial cell-bound HK and inhibit HK cleavage, PKa formation [38,39] as well as PKa-activated urokinase formation [40]. A 20 residue synthetic peptide (IQSDDDWIPDIQIDPNGLSF) derived from the HKD6 sequence was used to raise monoclonal antibody 3E8, which was shown to inhibit contact system activation by blocking the binding of PK and FXI to HK and additionally prevented downstream activation of FXII [41] (Figure 7B). A monoclonal antibody that has progressed into clinical development is 14E11, which binds to the FXI apple 2 domain and inhibits HK binding [42]. Recently, it has been shown that 14E11 improves venous thrombus resolution [43] and mitigates the development of experimental atherosclerosis [44].

Genomic studies have identified HKD6 missense variant rs710446 Ile563Thr (KNG1 Ile581Thr numbering with signal sequence included) as associated with a shortening of the activated partial thromboplastin time and increased susceptibility to venous thrombosis [45,46] (Figure 7B). The PK/FXI binding consequences of the HK Ile563Thr mutation are unknown, but the variant rs710446 is commonly found in human populations [45,46]. The Thr563 HK variant could introduce a new O-glycan site as HKD6 has multiple O-glycan sites [47]. The ~10-fold lower value of K_D obtained from the SPR measurements of the PK-HK peptide binding shown in Supplementary Table S1 compared with K_D from solution studies of peptides derived from cyanogen bromide cleavage of native HK protein fragments may be due to an O-glycan attached to HK Ser586 [47]. Figure 2C shows HK Ser586 hydroxyl hydrogen bonds to the Tyr143 side chain, and the addition of O-glycan residues may form addition interactions to the PK apple 2 domain Tyr143 and adjacent residues such as Lys111.

In terms of the structure of HKD6, our data show that 2 conformations of the HKD6 peptide exist when bound to FXI (straightened) or PK (bent double). The amino acid sequence of HKD6 is characterized as being rich in proline and acidic residues, which confers structural properties of a certain degree of rigidity as well as a negative charge. There is no structure for HKD6 alone and the Alphafold [48] program predicts an extended conformation of the polypeptide for both HKD5 and D6 with stretches of irregular regions punctuated by proline-rich helical structures. This extended HKD6 structure is likely important to project the HK polypeptide around the apple domain disc so the D4 domain can be brought into proximity with the PKa active site (Figure 7A).

The question remains as to why the FXI apple domain 1 domain does not bind HK. A thrombin-binding site has been identified in the apple 1 domain of FXI localized to Glu66, Lys83, and Gln84 [49], which is not present in PK and thus the apple 1 domain function may have shifted from binding HK to binding thrombin in FXI. In addition, the dimeric FXI places the 2 HK molecules in closer proximity, which may require an alternate conformation of HK (Figure 4A). An analysis of the evolutionary relationships of the FXI and PK genes [50] concluded that only PK and HK are present in lobe-finned fish, the ancestors of all land vertebrates. FXI arose later from a duplication of the PK gene early in mammalian evolution, and the FXI activation by thrombin is a more recent acquisition, appearing in placental mammals. Using the Alphafold program [48] with the sequences of both PKHC and HKD6, we attempted to ascertain whether the bent double conformation of HKpep1 is predicted for PK from *Xenopus laevis* (amphibian) where the FXI gene is absent. The Alphafold program predicted model of the *X. laevis* PK–HKpep1 complex is shown in Figure 7C, which has many features comparable to the human PKHC–HKpep1 complex (Figure 2C). This has the conserved features of the apple 1 domain β4–β5 loop and major pocket observed in human PK and key interactions with HK are maintained (Figure 7C). The *X. laevis* HKD6 peptide is slightly longer than the human equivalent, and this increase in length is also found in the *Latimeria chalumnae* sequence (lobe-finned fish), which is aligned in Figure 7D with conserved residues indicated.

ACKNOWLEDGMENTS

We acknowledge the Diamond Light Source for provision of synchrotron radiation in using the beamline I04. The crystal structures have been deposited in the Protein Data Bank (www.rcsb.org) with accession codes (PKHC–HKpep1, 7QOX and FXIHC–HKpep1, 7QOT). This work was supported by the British Heart Foundation Programme Grant no. RG/12/9/29775 to J.E., and grant 1702 from the Landsteiner Foundation for Blood Research to J.C.M.M.

AUTHOR CONTRIBUTIONS

J.E. and J.C.M.M. designed and supervised the study. C.L. generated the PKHC construct, performed cloning, protein expression and production, protein purification, crystallization, and structure solution. S.S.W. generated the FXIHC construct. C.L. and J.E. performed FXIHC protein crystallization, data collection, structure solution, model building and refinement. A.B.B. performed HDX–MS experiments. C.L. performed SPR experiments. J.E. prepared the figures, wrote the original draft manuscript with editing and review from all other authors. All authors conducted data analyses and interpretation. All authors revised and approved the final manuscript.

DECLARATION OF COMPETING INTERESTS

There are no competing interests to disclose.

REFERENCES

[1] Maas C, Oschatz C, Renne T. The plasma contact system 2.0. *Semin Thromb Hemost*. 2011;37:375–81. https://doi.org/10.1055/s-0031-1276586

[2] Schmaier AH. The contact activation and kallikrein/kinin systems: pathophysiologic and physiologic activities. *J Thromb Haemost*. 2016;14:28–39. https://doi.org/10.1111/jth.13194

[3] Schmaier AH. Antithrombotic potential of the contact activation pathway. *Curr Opin Hematol*. 2016;23:445–52. https://doi.org/10.1097/MOH.0000000000000271

[4] Long YM, Zhao XC, Clermont AC, Zhou QF, Liu Q, Feener EP, Yan B, Jiang GB. Negatively charged silver nanoparticles cause retinal vascular permeability by activating plasma contact system and disrupting adherens junction. *Nanotoxicology*. 2016;10:501–11. https://doi.org/10.3109/17435390.2015.1088589

[5] Irmscher S, Doring N, Halder LD, Jo EAH, Kopka I, Dunker C, Jacobsen ID, Luo S, Slevogt H, Lorkowski S, Beyersdorf N, Zipfel PF, Skerka C. Kallikrein cleaves C3 and activates complement. *J Innate Immun*. 2018;10:94–105. https://doi.org/10.1159/000484257

[6] Wuepper KD, Cochrane CG. Plasma prekallikrein: isolation, characterization, and mechanism of activation. *J Exp Med*. 1972;135:1–20. https://doi.org/10.1084/jem.135.1.1

[7] Papagrigoriou E, McEwan PA, Walsh PN, Emsley J. Crystal structure of the factor XI zymogen reveals a pathway for transactivation. *Nat Struct Mol Biol*. 2006;13:557–8. https://doi.org/10.1038/nsmb1095

[8] Hooley E, McEwan PA, Emsley J. Molecular modeling of the prekallikrein structure provides insights into high-molecular-weight kininogen binding and zymogen activation. *J Thromb Haemost*. 2007;5:2461–6. https://doi.org/10.1111/j.1538-7836.2007.02792.x

[9] Mandle RJ, Colman RW, Kaplan AP. Identification of prekallikrein and high-molecular-weight kininogen as a complex in human plasma. *Proc Natl Acad Sci U S A*. 1976;73:4179–83. https://doi.org/10.1073/pnas.73.11.4179

[10] Tans G, Rosing J, Berrettini M, Lammle B, Griffin JH. Autoactivation of human plasma prekallikrein. *J Biol Chem*. 1987;262:11308–14. https://doi.org/10.1016/S0021-9258(18)60960-3

[11] Bjorkqvist J, Jamsa A, Renne T. Plasma kallikrein: the bradykinin-producing enzyme. *Thromb Haemost*. 2013;110:399–407. https://doi.org/10.1160/TH13-03-0258

[12] Cichon S, Martin L, Hennies HC, Muller F, Van Driessche K, Karpushova A, Stevens W, Colombo R, Renne T, Drouet C, Bork K, Nothen MM. Increased activity of coagulation factor XII (Hageman factor) causes hereditary angioedema type III. *Am J Hum Genet*. 2006;79:1098–104. https://doi.org/10.1086/509899

[13] Simao F, Ustunkaya T, Clermont AC, Feener EP. Plasma kallikrein mediates brain hemorrhage and edema caused by tissue plasminogen activator therapy in mice after stroke. *Blood*. 2017;129:2280–90. https://doi.org/10.1182/blood-2016-09-740670

[14] Banerji A, Busse P, Shennak M, Lumry W, Davis-Lorton M, Wedner HJ, Jacobs J, Baker J, Bernstein JA, Lockey R, Li HH, Craig T, Cicardi M, Riedl M, Al-Ghazawi A, Soo C, Iarrobino R, Sexton DJ, TenHoor C, Kenniston JA, et al. Inhibiting plasma kallikrein for hereditary angioedema prophylaxis. *N Engl J Med*. 2017;376:717–28. https://doi.org/10.1056/NEJMoa1605767

[15] Kenniston JA, Faucette RR, Martik D, Comeau SR, Lindberg AP, Kopacz KJ, Conley GP, Chen J, Viswanathan M, Kastrapeli N, Cosic J, Mason S, DiLeo M, Abendroth J, Kuzmic P, Ladner RC, Edwards TE, TenHoor C, Adelman BA, Nixon AE, et al. Inhibition of plasma kallikrein by a highly specific active site blocking antibody. *J Biol Chem*. 2014;289:23596–608. https://doi.org/10.1074/jbc.M114.569061

[16] Liu J, Feener EP. Plasma kallikrein–kinin system and diabetic retinopathy. *Biol Chem*. 2013;394:319–28. https://doi.org/10.1515/hsz-2012-0316

[17] Teufel DP, Bennett G, Harrison H, van Rietschoten K, Pavan S, Stace C, Le Floch F, Van Bergen T, Vermassen E, Barbeaux P, Hu TT, Feyen JHM, Vanhove M. Stable and long-lasting, novel bicyclic peptide plasma kallikrein inhibitors for the treatment of diabetic macular edema. *J Med Chem*. 2018;61:2823–36. https://doi.org/10.1021/acs.jmedchem.7b01625

[18] Stefanini AC, da Cunha BR, Henrique T, Tajara EH. Involvement of kallikrein-related peptidases in normal and pathologic processes. *Dis Markers*. 2015;2015:946572. https://doi.org/10.1155/2015/946572

[19] Colman RW, Wachtfogel YT, Kucich U, Weinbaum G, Hahn S, Pixley RA, Scott CF, de Agostini A, Burger D, Schapira M. Effect of cleavage of the heavy chain of human plasma kallikrein on its functional properties. *Blood*. 1985;65:311–8. https://doi.org/10.1182/blood.V65.2.311.311

[20] Herwald H, Jahnen-Dechent W, Alla SA, Hock J, Bouma BN, Muller-Esterl W. Mapping of the high molecular weight kininogen binding site of prekallikrein. Evidence for a discontinuous epitope formed by distinct segments of the prekallikrein heavy chain. *J Biol Chem*. 1993;268:14527–35. https://doi.org/10.1016/S0021-9258(19)85270-5

[21] Renne T, Sugiyama A, Gailani D, Jahnen-Dechent W, Walter U, Muller-Esterl W. Fine mapping of the H-kininogen binding site in plasma prekallikrein apple domain 2. *Int Immunopharmacol*. 2002;2:1867–73. https://doi.org/10.1016/s1567-5769(02)00170-4

[22] Winn MD, Ballard CC, Cowtan KD, Dodson EJ, Emsley P, Evans PR, Keegan RM, Krissinel EB, Leslie AG, McCoy A, McNicholas SJ, Murshudov GN, Pannu NS, Potterton EA, Powell HR, Read RJ, Vagin A, Wilson KS. Overview of the CCP4 suite and current developments. *Acta Crystallogr D Biol Crystallogr*. 2011;67:235–42. https://doi.org/10.1107/S0907444910045749

[23] McCoy AJ, Grosse-Kunstleve RW, Adams PD, Winn MD, Storoni LC, Read RJ. Phaser crystallographic software. *J Appl Crystallogr*. 2007;40:658–74. https://doi.org/10.1107/S0021889807021206

[24] Emsley J, McEwan PA, Gailani D. Structure and function of factor XI. *Blood*. 2010;115:2569–77. https://doi.org/10.1182/blood-2009-09-199182

[25] Laskowski RA, Swindells MB. LigPlot+: multiple ligand–protein interaction diagrams for drug discovery. *J Chem Inf Model*. 2011;51:2778–86. https://doi.org/10.1021/ci200227u

[26] Tait JF, Fujikawa K. Primary structure requirements for the binding of human high molecular weight kininogen to plasma prekallikrein and factor XI. *J Biol Chem*. 1987;262:11651–6. https://doi.org/10.1016/S0021-9258(18)60859-2

[27] Joseph K, Kaplan AP. Formation of bradykinin: a major contributor to the innate inflammatory response. *Adv Immunol*. 2005;86:159–208. https://doi.org/10.1016/S0065-2776(04)86005-X

[28] Li C, Voos KM, Pathak M, Hall G, McCrae KR, Dreveny I, Li R, Emsley J. Plasma kallikrein structure reveals apple domain disc rotated conformation compared to factor XI. *J Thromb Haemost*. 2019;17:759–70. https://doi.org/10.1111/jth.14418

[29] Wong SS, Ostergaard S, Hall G, Li C, Williams PM, Stennicke H, Emsley J. A novel DFP tripeptide motif interacts with the coagulation factor XI apple 2 domain. *Blood*. 2016;127:2915–23. https://doi.org/10.1182/blood-2015-10-676122

[30] Baglia FA, Gailani D, Lopez JA, Walsh PN. Identification of a binding site for glycoprotein Ibalpha in the Apple 3 domain of factor XI. *J Biol Chem*. 2004;279:45470–6. https://doi.org/10.1074/jbc.M406727200

[31] Bar Barroeta A, van Galen J, Stroo I, Marquart JA, Meijer AB, Meijers JCM. Hydrogen–deuterium exchange mass spectrometry highlights conformational changes induced by factor XI activation and binding of factor IX to factor XIa. *J Thromb Haemost*. 2019;17:2047–55. https://doi.org/10.1111/jth.14632

[32] Kelley LA, Mezulis S, Yates CM, Wass MN, Sternberg MJ. The Phyre2 web portal for protein modeling, prediction and analysis. *Nat Protoc*. 2015;10:845–58. https://doi.org/10.1038/nprot.2015.053

[33] Muller JJ, Weiss MS, Heinemann U. PAN-modular structure of microneme protein SML-2 from the parasite *Sarcocystis muris* at 1.95 Å resolution and its complex with 1-thio-beta-D-galactose. *Acta Crystallogr D Biol Crystallogr*. 2011;67:936–44. https://doi.org/10.1107/s0907444911037796

[34] Gailani D, Geng Y, Verhamme I, Sun MF, Bajaj SP, Messer A, Emsley J. The mechanism underlying activation of factor IX by factor XIa. *Thromb Res*. 2014;133:S48–51. https://doi.org/10.1016/j.thromres.2014.03.020

[35] Sun Y, Gailani D. Identification of a factor IX binding site on the third apple domain of activated factor XI. *J Biol Chem*. 1996;271:29023–8. https://doi.org/10.1074/jbc.271.46.29023

[36] Sun MF, Zhao M, Gailani D. Identification of amino acids in the factor XI apple 3 domain required for activation of factor IX. *J Biol Chem*. 1999;274:36373–8. https://doi.org/10.1074/jbc.274.51.36373

[37] Geng Y, Verhamme IM, Sun MF, Bajaj SP, Emsley J, Gailani D. Analysis of the factor XI variant Arg184Gly suggests a structural basis for factor IX binding to factor XIa. *J Thromb Haemost*. 2013;11:1374–84. https://doi.org/10.1111/jth.12275

[38] Vogel R, Kaufmann J, Chung DW, Kellermann J, Müller-Esterl W. Mapping of the prekallikrein-binding site of human H-kininogen by ligand screening of lambda gt11 expression libraries. Mimicking of the predicted binding site by anti-idiotypic antibodies. *J Biol Chem*. 1990;265:12494–502. https://doi.org/10.1016/S0021-9258(19)38373-5

[39] Joseph K, Tholanikunnel BG, Kaplan AP. Factor XII-independent cleavage of high-molecular-weight kininogen by prekallikrein and inhibition by C1 inhibitor. *J Allergy Clin Immunol*. 2009;124:143–9. https://doi.org/10.1016/j.jaci.2009.02.006

[40] Lin Y, Harris RB, Yan W, McCrae KR, Zhang H, Colman RW. High molecular weight kininogen peptides inhibit the formation of kallikrein on endothelial cell surfaces and subsequent urokinase-

dependent plasmin formation. *Blood*. 1997;90:690–7. https://doi.org/10.1182/blood.V90.2.690

[41] Chen ZL, Singh PK, Horn K, Strickland S, Norris EH. Anti-HK antibody reveals critical roles of a 20-residue HK region for Aβ-induced plasma contact system activation. *Blood Adv*. 2022;6:3090–101. https://doi.org/10.1182/bloodadvances.2021006612

[42] Cheng Q, Tucker EI, Pine MS, Sisler I, Matafonov A, Sun MF, White-Adams TC, Smith SA, Hanson SR, McCarty OJ, Renné T, Gruber A, Gailani D. A role for factor XIIa-mediated factor XI activation in thrombus formation in vivo. *Blood*. 2010;116:3981–9. https://doi.org/10.1182/blood-2010-02-270918

[43] Jordan KR, Wyatt CR, Fallon ME, Woltjer R, Neuwelt EA, Cheng Q, Gailani D, Lorentz C, Tucker EI, McCarty OJT, Hinds MT, Nguyen KP. Pharmacological reduction of coagulation factor XI reduces macrophage accumulation and accelerates deep vein thrombosis resolution in a mouse model of venous thrombosis. *J Thromb Haemost*. 2022;20:2035–45. https://doi.org/10.1111/jth.15777

[44] Ngo ATP, Jordan KR, Mueller PA, Hagen MW, Reitsma SE, Puy C, Revenko AS, Lorentz CU, Tucker EI, Cheng Q, Hinds MT, Fazio S, Monia BP, Gailani D, Gruber A, Tavori H, McCarty OJT. Pharmacological targeting of coagulation factor XI mitigates the development of experimental atherosclerosis in low-density lipoprotein receptor-deficient mice. *J Thromb Haemost*. 2021;19:1001–17. https://doi.org/10.1111/jth.15236

[45] Morange PE, Oudot-Mellakh T, Cohen W, Germain M, Saut N, Antoni G, Alessi MC, Bertrand M, Dupuy AM, Letenneur L, Lathrop M, Lopez LM, Lambert JC, Emmerich J, Amouyel P, Trégouët DA. KNG1 Ile581Thr and susceptibility to venous thrombosis. *Blood*. 2011;117:3692–4. https://doi.org/10.1182/blood-2010-11-319053

[46] Houlihan LM, Davies G, Tenesa A, Harris SE, Luciano M, Gow AJ, McGhee KA, Liewald DC, Porteous DJ, Starr JM, Lowe GD, Visscher PM, Deary IJ. Common variants of large effect in F12, KNG1, and HRG are associated with activated partial thromboplastin time. *Am J Hum Genet*. 2010;86:626–31. https://doi.org/10.1016/j.ajhg.2010.02.016

[47] Hoffmann M, Marx K, Reichl U, Wuhrer M, Rapp E. Site-specific O-glycosylation analysis of human blood plasma proteins. *Mol Cell Proteomics*. 2016;15:624–41. https://doi.org/10.1074/mcp.M115.053546

[48] Jumper J, Evans R, Pritzel A, Green T, Figurnov M, Ronneberger O, Tunyasuvunakool K, Bates R, Žídek A, Potapenko A, Bridgland A, Meyer C, Kohl SAA, Ballard AJ, Cowie A, Romera-Paredes B, Nikolov S, Jain R, Adler J, Back T, et al. Highly accurate protein structure prediction with AlphaFold. *Nature*. 2021;596:583–9. https://doi.org/10.1038/s41586-021-03819-2

[49] Baglia FA, Walsh PN. A binding site for thrombin in the apple 1 domain of factor XI. *J Biol Chem*. 1996;271:3652–8. https://doi.org/10.1074/jbc.271.7.3652

[50] Ponczek MB, Shamanaev A, LaPlace A, Dickeson SK, Srivastava P, Sun MF, Gruber A, Kastrup C, Emsley J, Gailani D. The evolution of factor XI and the kallikrein–kinin system. *Blood Adv*. 2020;4:6135–47. https://doi.org/10.1182/bloodadvances.2020002456

SUPPLEMENTARY MATERIAL

The online version contains supplementary material available at https://doi.org/10.1016/j.jtha.2023.03.042